metals

MDPI

Article

Simulation and Experimental Study on Jet Velocity of Zr-Based Amorphous Alloy Liner

Ping Cui, Xinbao Gao, Jingqing Xu, Jian Wen *, Liang Cui, Chaowang Li and Yanfeng Yang

Shijiazhuang Campus, Army Engineering University of PLA, Shijiazhuang 050003, China; pingjing1981@163.com (P.C.); cctv2004re@163.com (X.G.); xujingqing1983@163.com (J.X.); cuiliang_1980_sx@163.com (L.C.); lichaowangzxz@163.com (C.L.); yyfhbs@sohu.com (Y.Y.)
* Correspondence: wenjian19740719@163.com; Tel.:+860-311-8799-4316

Abstract: Zr-based amorphous alloy is a new energetic material that has been closely monitored and extensively studied for the design of highly effective shaped charge warheads in recent years. In order to accurately determine the motion parameters of shaped charge jets during the detonation-driven formation process of Zr-based amorphous alloy liners, we prepared conical ZrCuNiAlAg liners by vacuum die casting and supercooled liquid high-rheological-rate formation processes. Based on jet-formation numerical simulation, pulsed X-ray imaging and copper foil target velocity measuring tests were conducted to identify the variation trend of the jet velocity of Zr-based amorphous alloy liners with time. The jet velocities at typical moments in the free flight stage were verified. The research results showed that Zr-based amorphous alloy liners could produce solid jets, whose velocity was in gradient descent from the head to the tail, and that the jet's head velocity peaked at 12 μs and then slowly decreased with time. The average velocities measured by the X-ray imaging and copper foil target tests were 6913 m/s and 7177 m/s, respectively, and both of them were in good agreement with the simulation results, verifying the accuracy of the numerical simulation model for jet formation. The formation processes of shaped charge liners were found to affect the mechanical properties of the material and thus, the jet's formation process and motion parameters. The Zr-based amorphous alloy liner formed by the supercooled liquid-phase high-rheological-rate formation process exhibited a jet velocity 6.5% higher than that formed by the vacuum die casting process.

Keywords: Zr-based amorphous alloy; Mohaupt effect; jet velocity; pulsed X-ray imaging; copper foil target velocity measuring

check for updates

Citation: Cui, P.; Gao, X.; Xu, J.; Wen, J.; Cui, L.; Li, C.; Yang, Y. Simulation and Experimental Study on Jet Velocity of Zr-Based Amorphous Alloy Liner. *Metals* **2022**, *12*, 978. https://doi.org/10.3390/met12060978

Academic Editors: Xianfeng Zhang and Zhongwei Guan

Received: 5 May 2022
Accepted: 1 June 2022
Published: 7 June 2022

Publisher's Note: MDPI stays neutral with regard to jurisdictional claims in published maps and institutional affiliations.

Copyright: © 2022 by the authors. Licensee MDPI, Basel, Switzerland. This article is an open access article distributed under the terms and conditions of the Creative Commons Attribution (CC BY) license (https://creativecommons.org/licenses/by/4.0/).

1. Introduction

The liner is the core component of shaped charges. The detonation of the explosive charge crushes and closes the liner under the Mohaupt effect to form a high-velocity jet that can penetrate the target. The motion parameters of jets are of great significance to their damage performance, such as penetration depth. According to the ideal and incompressible fluid dynamics [1], the larger the ratio of the jet's head to tail velocity, the greater the penetration depth. The shape of a jet is also closely associated with its velocity, and the head-to-tail velocity gradient is the primary cause of jet formation. In order to study the formation behavior of jets and their damageability, it is necessary to accurately determine jet velocity and its variation law.

In addition to numerical simulation, the commonly-used experimental methods for jet velocity measurement include pulsed X-ray imaging and closed switch circuit. Ref. [2] captured the instantaneous shape of copper and steel jets and calculated their velocities to be 5535 m/s and 5275 m/s, respectively, using the pulsed X-ray imaging method but failed to obtain X-ray images of the low-density aluminum jet. Ref. [3] studied the formation behavior of copper jets by a double-layered shaped charge using a dual-channel 450 kV Scandi flash X-ray system that could capture the real shapes of copper jets at two different

light-emitting moments. The error between the measurement and simulation results was found to be less than 6%. Refs. [4–7] are some similar studies that applied X-ray imaging to jet velocity measurement.

Pulsed X-ray imaging calculates the jet velocity by capturing the shapes and positions of the jet at different moments, but it has the disadvantages of complex equipment, high cost, and poor performance for low-density jets. Comparatively, the closed switch circuit method requires simple velocity-measuring equipment and boasts such advantages as a low cost, high efficiency, and freedom from the influence of jet materials. More importantly, the method enables the measurement of jet velocities during free flight and target penetration. Ref. [8] measured the residual velocity of steel, copper, and aluminum jets after penetrating a spaced multi-layer concrete target using multiple sheets of aluminum foils. Ref. [9] measured the residual velocity of copper jets after penetrating a woven-fabric-reinforced rubber composite target using copper foils. In order to investigate the penetrability of the aluminum jet to loose and dense sand targets, Ref. [10] set up a multi-layer closed switch in the sandbox and measured the real-time velocity of the aluminum jet in sand of different densities. Ref. [11] used copper wire mesh as a switch and measured the velocity of a hyperboloidal explosively formed projectile to be 1914 m/s. The above studies show that both the methods are effective for jet velocity measurement.

Driven by the military demand for high-efficiency damage, energetic liner materials have become a research hotspot in the field of shaped charges in recent years. Zr-based amorphous alloys, new energetic structural materials that have enjoyed rapid development over the years, have attracted extensive attention. Studies have shown that Zr-based amorphous alloys undergo violent energy-release reactions under high dynamic loading conditions [12–15], causing high damage as a result of kinetic and chemical energy superposition. Under the action of shaped charge detonation, the kinetic energy of the jet combines with the violent chemical reaction of the amorphous material. While penetrating the target, the jet produces such damaging behaviors as secondary explosion, heat release, and combustion. These behaviors can significantly enhance the comprehensive damage performance of shaped-charge penetrators.

To date, there have been few studies on the application of Zr-based amorphous alloy materials in the shaped-charge field. Laszlo and William [16] from the U.S. Army Research Laboratory Weapons and Materials Research Directorate (WMRD), for the first time, performed X-ray imaging at the Aberdeen Proving Ground for the shape of a jet during the free flight stage; it was formed from a conical ZrNbCuNiAl amorphous alloy liner produced by Howmet Corporation, using an injection molding process. The results of the two imaging tests showed that the jet from Zr-based amorphous alloy liners was generally powdery and shared similar characteristics with typical shaped-charge jets formed from a powder metallurgy material liner. Refs. [17–19] numerically simulated and experimentally studied the formation process and penetration properties of jets from Zr-based amorphous alloy liners. However, they failed to systematically investigate their motion parameters, let alone the effects of the liners' material production process on the parameters.

Therefore, this paper preliminarily worked out the flight velocity and variation law of jets from Zr-based amorphous alloy liners using numerical simulation software. In addition, the jet velocity was verified with two methods, namely, pulsed X-ray imaging and copper foil target velocity measurement. Considering the effects of material processing techniques on jet motion parameters, this paper conducted contrast tests using two Zr-based amorphous alloy liners separately formed by vacuum die casting and supercooled liquid-phase high rheology. The research work is expected to provide a scientific basis and engineering reference for the study of the damage performance of jets from Zr-based amorphous alloy liners.

2. Numerical Simulation

2.1. Finite Element Model

The shaped-charge structure was composed of a liner, an explosive, and a shell. One end of the cylindrical explosive was provided with a conical hole in which to place the conical liner. The length of the explosive column was 64.7 mm, and its diameter was the same as the outer diameter of the mouth of the liner. The material of the liner was quintary amorphous alloys $Zr_{63.5}Cu_{12}Ni_{10}Al_{12.5}Ag_2$ (atomic percentage) or $Zr_{75.28}Cu_{9.91}Ni_{7.63}Al_{4.38}Ag_{2.8}$ (mass percentage). The shell was made of aluminum, with a thickness of 2.9mm. The models of the components were built separately by 3D modeling software. The detonation method of the shaped charge was single-point detonation. With ANSYS Autodyn software (19.0.0.2017113019, Century Dynamics, Fort Worth, TX, USA), an air domain with a size of 550 mm × 60 mm was created to calculate the large-deformation flow field during the shaped-charge jet formation process. Since the Euler method can effectively solve multi-material flow problems under the conditions of high strain and high strain rates, the Euler mesh was used for jet-formation simulation. Considering the symmetry of the jet-formation process, a two-dimensional axisymmetric calculation model was employed so as to reduce the computational workload and boost the simulation efficiency. In order to eliminate boundary effects, the air domain boundary condition was set to "Flow_Out", and the constructed finite element model for numerical simulation is shown in Figure 1.

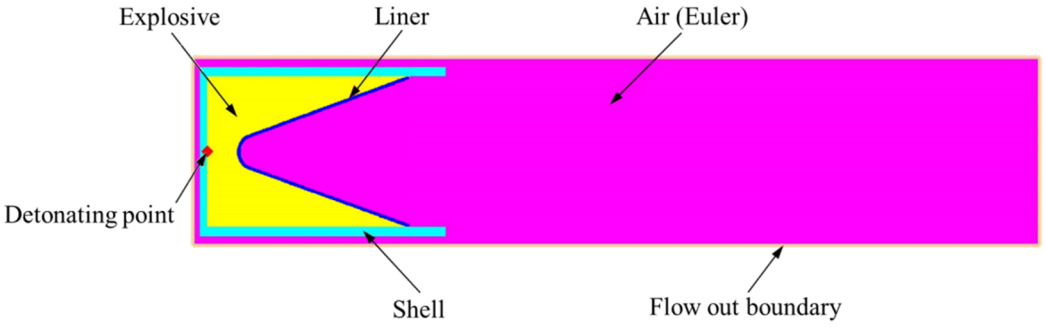


Figure 1. The finite element model.

2.2. Material Model and Equation of State

In the simulation, the explosive 8701 was used, with a density of 1.713 g/cm^3 and a detonation velocity of 7980 m/s. The detonation gas expansion process was described by the JWL equation of state (EOS), and the main parameters of the material are shown in Table 1. The liner was made of ZrCuNiAlAg amorphous alloys, and the polynomial EOS in the JH-2 model was adopted. The material parameters of the liner are shown in Table 2. The shaped-charge shell was made of AL 2024-T4 in the Autodyn material library, and the Shock EOS was used. The material parameters of the shell are shown in Table 3. The Euler domain was filled with air, and its state equation was the ideal gas EOS. The parameters of the air are shown in Table 4.

Table 1. Material parameters of the 8701 explosive [20,21].

Parameters	Density ρ/g·cm^{-3}	D_{CJ}/m·s^{-1}	P_{CJ}/GPa	E_{CJ}/(KJ/m^3)	A/GPa	B/GPa	R_1	R_2	ω
Values	1.713	7980	28.6	8.499×10^6	524.23	7.768	4.2	1.1	0.34

Table 2. JH-2 material parameters of ZrCuNiAlAg amorphous alloy [22].

Parameters	Density ρ/g·cm^{-3}	A_1 /GPa	A_3 /kPa	G /GPa	B	M	D_1	σ_{HEL} /GPa	A_2 /kPa	T_1 /GPa	A	C	N	D_2
Values	6.581	2303	8.873×10^{11}	3.704	1.03	0.383	0.005	5.82	4.716×10^{10}	2303	0.296	0.094	1.153	1

Table 3. Material parameters of AL 2024-T4 [23].

Parameters	Density ρ /g·cm^{-3}	Gruneisen Coefficient	C_1/m·s^{-1}	S_1	Specific Heat /(J/kgK)
Values	2.785	2	5328	1.338	863.000061

Table 4. Material parameters of AIR [21].

Parameters	Density ρ /g·cm^{-3}	γ	C_P/(kJ/kg·K)	C_V /(kJ/kg·K)	T/K	E_0 /(kJ/kg^{-1})
Values	1.225	1.4	1.005	0.718	288.2	2.068×10^5

2.3. Simulation Results and Discussion

Figure 2 shows the shape variations of the jet from the conical liner with time (0~40 μs). As illustrated, the jet-formation process of Zr-based amorphous alloy liners involves the stages of normal crushing, axial closing, centerline collision, extrusion stretching, etc., while a formed jet consists of the head and the slug. As time progresses, the tail fins on both sides of the jet that are evolved from the generatrix of the liner gradually become shorter and are largely transformed into the head and slug of the jet. As a result, the jet is stretched and elongated with time. The diameter of the slug does not change significantly with time, but the head exhibits discrete phenomena such as bifurcation and hollowness during free flight.

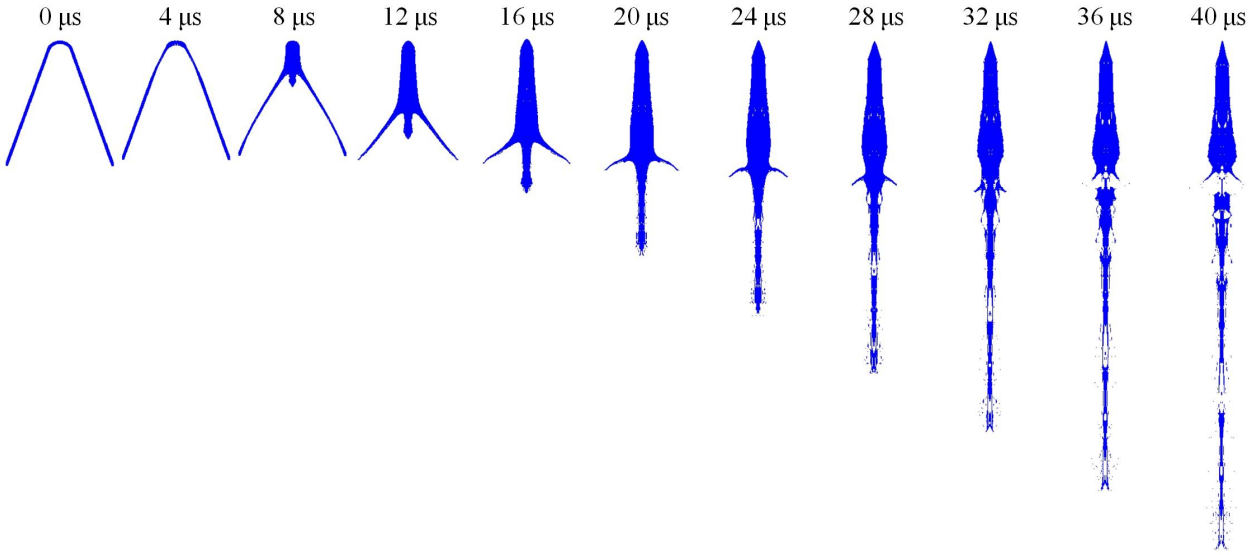


Figure 2. Shape variations of the jet from the conical liner with time.

The velocity of the jet's head represents its penetration capability to some extent. Figure 3 presents the velocity variations of the head of the jet from a conical Zr-based amorphous alloy liner with time during the period of 0–40 μs, given by simulation. Figure 4 presents the cloud diagram of the jet's velocity distribution at the moment of 30 μs.

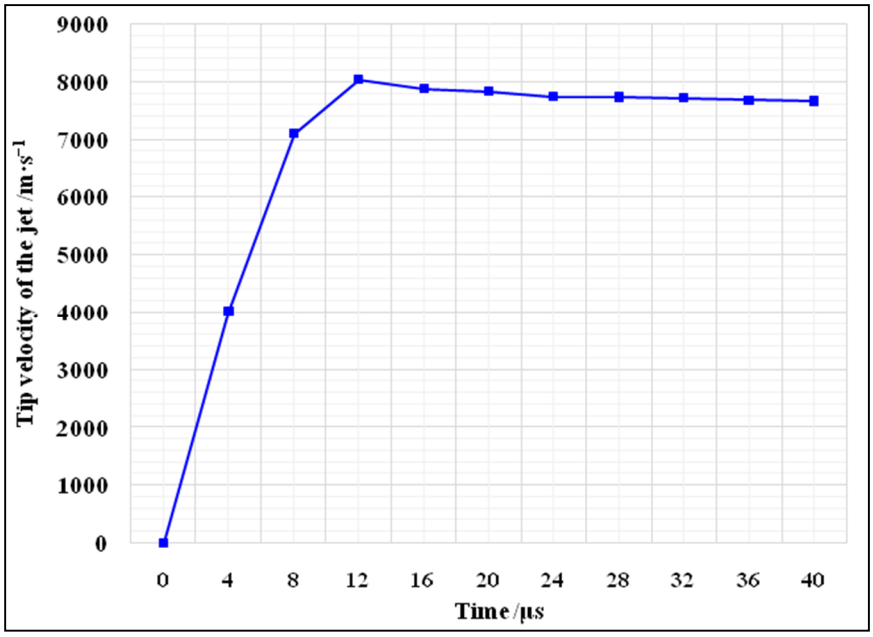


Figure 3. The head-velocity variations of the jet with time during the period of 0–40 μs.

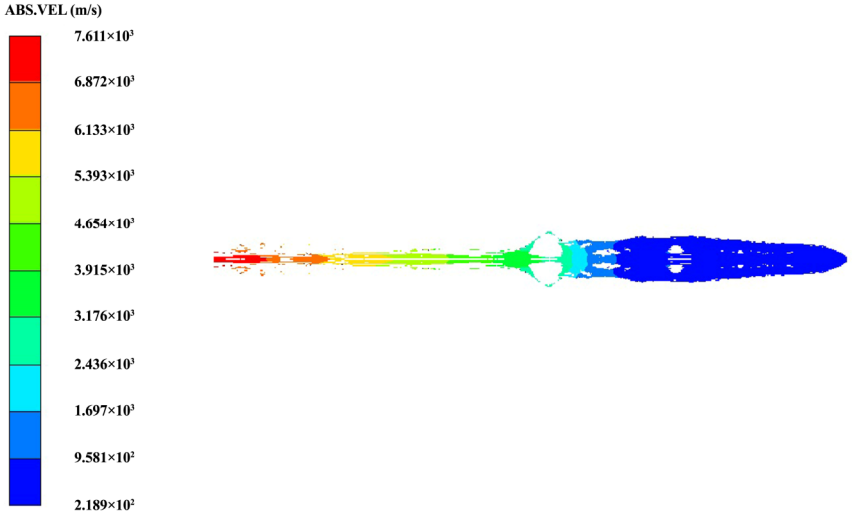


Figure 4. The cloud diagram of the jet's velocity distribution at the moment of 30 μs.

The simulation results showed that the velocity of the jet decreased gradually from the head to the tail, and the head-to-tail velocity gradient was the reason for the stretching and elongation of the jet. The velocity of the jet's head rapidly increased to a maximum value of 8026 m/s within 0–12 μs and then decreased slowly within 12–40 μs. At 40 μs, the head velocity was 7655 m/s, less than 0.67% lower than 7707 m/s at 30 μs.

3. Pulsed X-ray Imaging Test

Shaped-charge jets feature high velocity (usually in the range of 5000–8000 m/s), small volume (mostly 10–20cm in length and no more than 10 mm in diameter), and poor motion environment (with detonation products around). Hence, the effective method commonly used for capturing the shape of high-density metal jets is pulsed X-ray imaging [24–26].

3.1. Test Principle

The working principle of the pulsed X-ray imaging for jets is shown in Figure 5. The shaped charge is placed on a low-density plastic height of burst (HOB) cylinder with a

certain length, so that it is between the two light outlets of the X-ray machine and their corresponding cassettes at the same time. A cylinder with an appropriate height is selected to ensure that the jet can be completely projected onto both cassettes. A thin iron wire is pasted along the horizontal direction at the appropriate position of each cassette, and its X-ray projection can be used as the reference line for subsequent jet-motion parameter measurement. The timing device of the X-ray machine starts when the shaped charge is detonated, and the light-emitting time is adjustable within a wide range according to the needs of jet observation. It can be seen from Figure 5a that X_1 is the horizontal distance from the metal jet to the light outlet and that X_2 is the horizontal distance from the metal jet to the cassette. Apparently, the jet's X-ray projection has an enlarged size with respect to the original jet. The ratio of the size of the jet in the X-ray image to the real size of the jet is called magnification, denoted as K. According to the principle of geometric similarity, $K = (X_1 + X_2)/X_1$.

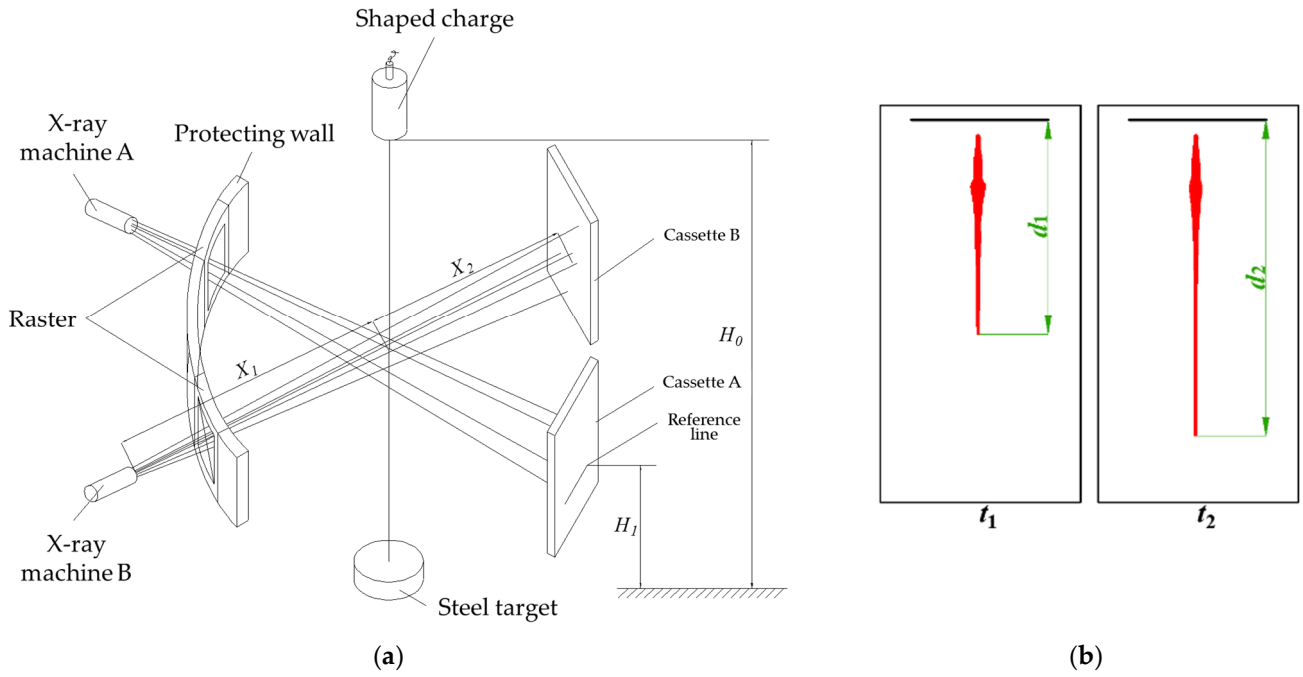


Figure 5. The working-principle diagram of the pulsed X-ray imaging for jets: (**a**) location relationship of the instruments and (**b**) the calculation principle for jet velocity.

According to the position of the reference line on the film, the size of the jet d and the light-emitting time of the two X-ray machines t_1 and t_2, and in consideration of the magnification, the jet's head velocity can be given by $V_j = (d_2 - d_1)/(t_2 - t_1)$.

3.2. Test Scheme

The pulsed X-ray imaging test for the jet from a Zr-based amorphous alloy liner was carried out in a dedicated explosion tower with radiation protection. Figure 6a is the X-ray light-emitting controller, and Figure 6b is the layout of the test site. During the test, the light-emitting time of the X-ray controllers was uniformly set, with channels A and B to be 30 μs and 40 μs, respectively.

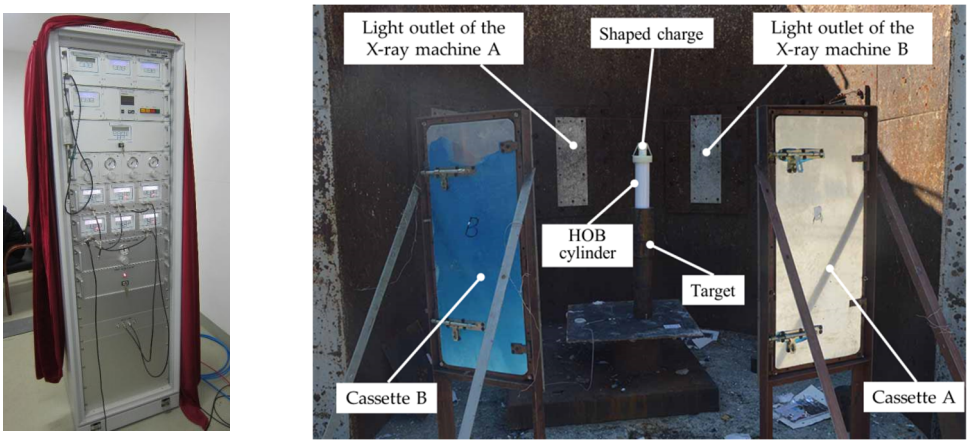


Figure 6. The layout of the X-ray imaging test: (**a**) the X-ray light-emitting controller and (**b**) the layout of the test site.

The test consumed two conical shaped-charge liners made of Zr-based amorphous alloys but by different formation processes, namely, vacuum die-casting and supercooled liquid phase high rheology. The explosive 8701, installed by no-liner pressing, was used as the shaped charge with a density of about 1.79 g/cm^3. The booster column, in size of $\Phi 15 \times 7$ mm, was made of pressed and passivated Hexogen. In order to prevent the metal fragments generated by the explosion from damaging the light outlets of the X-ray machine, a nylon shell was employed for the shaped charge. The height of the HOB cylinder was set to 300 mm so as to fully stretch the formed jet and accomplish the X-ray imaging twice. The test liners and the real shaped charges are shown in Figure 7, and the parameters of the shaped charges are listed in Table 5.



Figure 7. Photographs of the liners and shaped charges: (**a**) the liners, (**b**) the shaped charges, and (**c**) the assembly relationship and location of the shaped charges.

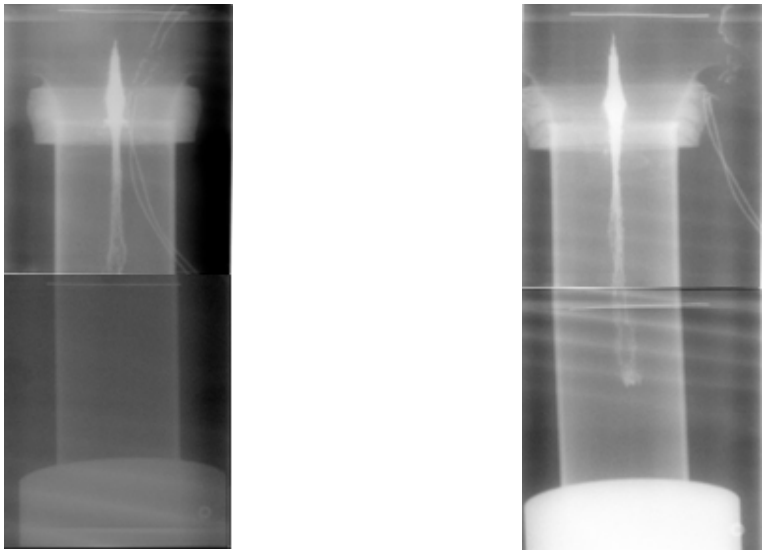
Table 5. Parameters of the shaped charges.

Number of the Liners	Formation Processes of the Liners	Mass of the Liners/g	Mass of the Shaped Charges/g	Height of the Shaped Charges/mm
S3	the vacuum die casting process	42.0	190.0	64.6
H4	the supercooled liquid-phase high-rheological-rate formation process	38.4	186.5	64.7

3.3. Test Results

For the shaped charge numbered S3, the actual light-emitting time of channel A was 31.082 μs; at the time, the lengths of the jet's head and slug were 104.34 and 62.1 mm, respectively. The actual light-emitting time of channel B was 40.701 μs, and at the time, their lengths were 179.93 and 60.42 mm. Figure 8 shows the X-ray images of the jet captured

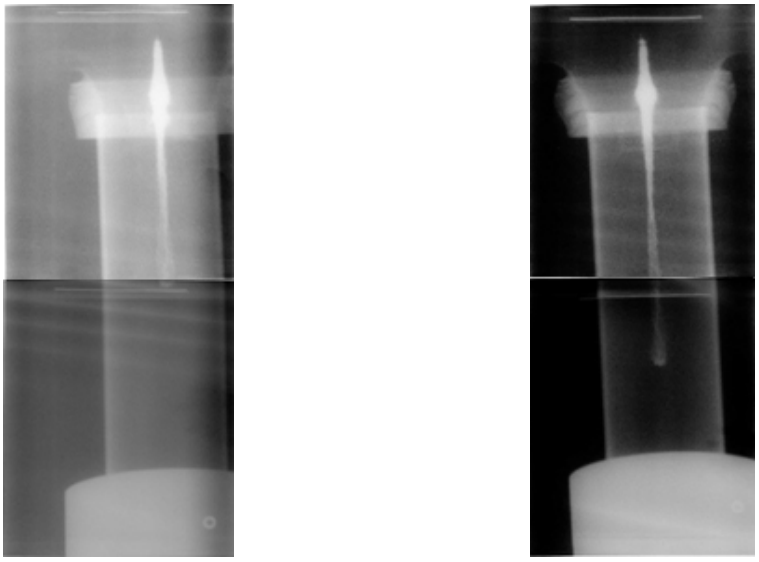
by the light outlets A and B. After equivalent conversion, the velocity of the jet's head was obtained to be 6710 m/s.



(**a**) (**b**)

Figure 8. X-ray image of the Zr-based amorphous alloy jet (S3): (**a**) captured by the light outlet A at 31.082 μs and (**b**) captured by the light outlet B at 40.701 μs.

For the shaped charge numbered H4, the actual light-emitting time of channel A was 32.748 μs; at the time, the lengths of the jet's head and slug were 117.44 and 58.13 mm, respectively. The actual light-emitting time of channel B was 40.802 μs, and at the time, their lengths were 181.85 and 55.9 mm. Figure 9 shows the X-ray images of the jet captured by the light outlets A and B. After equivalent conversion, the velocity of the jet's head was obtained to be 7116 m/s.



(**a**) (**b**)

Figure 9. X-ray image of the Zr-based amorphous alloy jet (H4): (**a**) captured by light outlet A at 32.748 μs and (**b**) captured by light outlet B at 40.802 μs.

4. Copper Foil Target Velocity Measuring Test

The copper foil target velocity measuring system consists of copper foil target and a velocimeter, and its working principle is shown in Figure 10a. On each of the cylindrical end face of the HOB cylinder is a target sheet, which is connected with the NLG202-Z dual-channel velocimeter. The shaped charge is remotely detonated by a detonator and the formed-jet perforates the two target sheets in order. The difference in perforation time between the two target sheets on the end faces was the time the jet's head takes to pass through the HOB cylinder, and it is given in real time by the velocimeter. According to the height of the HOB cylinder and the time difference, the average velocity of the head can be calculated. The site layout of the velocity-measuring system is shown in Figure 10b.

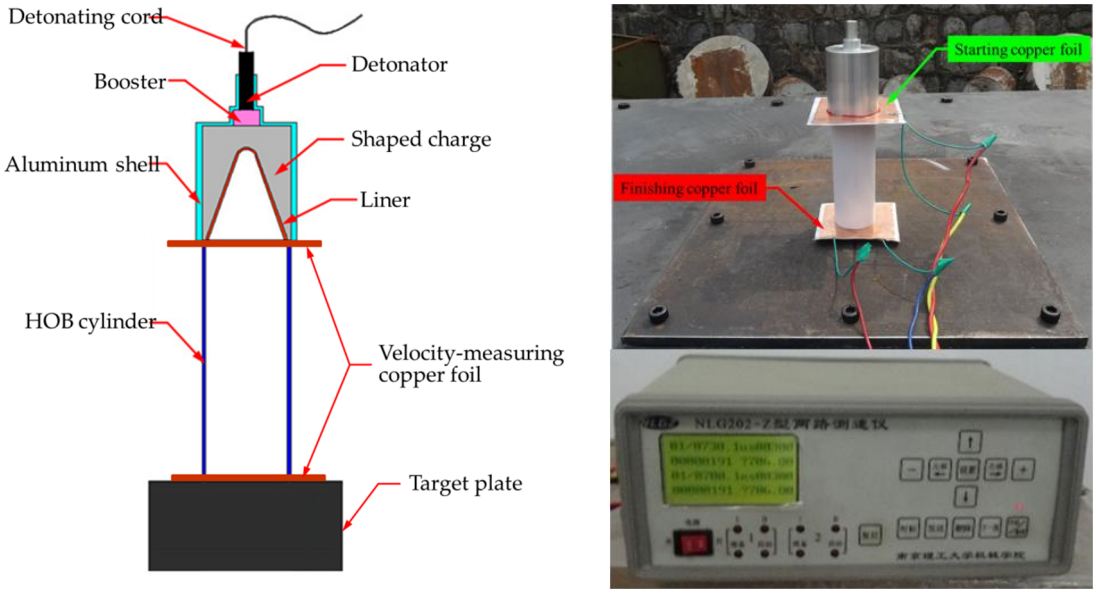


Figure 10. The copper foil target velocity measuring system: (**a**) sketch map of working principle and (**b**) the site layout of the system.

Table 6 presents the time the jets pass through the two targets sheets and their calculated velocities for the two Zr-based amorphous alloy liners produced by different formation processes. It can be seen that the average velocity of the jets is 7177 m/s. With regard to the effect of formation processes, the jet formed by supercooled liquid-phase high rheology has a velocity 7.0% higher than the jet formed by vacuum die casting.

Table 6. Test results of copper foil target velocity-measuring system.

Number of the Liners	Forming Processes of Liners	Height of the HOBCylinder/mm	Time Passing through/μs	Jet Velocity/m·s^{-1}
S10	the vacuum die casting process	138	19.9	6935
H6	the supercooled liquid-phase high-rheological-rate formation process	138	18.6	7419

5. Error Analysis

As described above, the jet velocities were obtained by simulation and testing. The results showed that the jet velocities obtained by simulating calculation and pulsed X-ray imaging were the largest and the smallest, respectively, and the velocity given by the copper foil target velocity-measuring test was in between. According to the working principle,

the jet velocity measured by the copper foil target velocity-measuring test was the average velocity of the jet from the liner mouth (about 14 μs) to the target (about 34 μs); the velocity measured by the pulsed X-ray imaging test was the average velocity during the period 30–40 μs. As illustrated by the variation curve of the jet velocity with time in Figure 3, the jet velocity measured by the copper foil target test was 7177 m/s, 3.8% higher than the 6913 m/s measured by the pulsed X-ray imaging test. Additionally, in the copper foil target velocity-measuring test, the shell of the shaped-charge was made of aluminum, but in the pulsed X-ray imaging test, its material used was nylon. Hence, the shell strength would also be responsible for the velocity difference measured by the two methods.

The velocity of the jet's head measured by the copper foil target velocity-measuring test was 7.3% lower than the simulation result, i.e., 7740 m/s at 24 μs. The velocity measured by the pulsed X-ray imaging test was 9.9% lower than the simulation result, i.e., 7672 m/s at 36 μs.The numerical simulation showed a jet velocity higher than the values given by both the tests. This should be ascribed to the fact that the numerical simulation calculation model and material parameters are of idealization. However, in actual tests, factors such as explosive density, liner structural symmetry, and errors from test instruments are not neglectable. On the whole, the jet velocity given by the copper foil target velocity-measuring test was in good agreement with the simulation result. It is also worth noting that the numerical simulation model previously built for jet formation and the material model used exhibited satisfactory accuracy.

With regard to mechanical properties, the Zr-based amorphous alloy liner produced by vacuum die casting exhibits brittleness, but that produced by supercooled liquid-phase high rheology takes on better room-temperature plasticity. Consequently, in the copper foil target velocity-measuring test, the jet formed from the plastic liner was found to have a velocity 7.0% higher than that from the brittle liner; in the pulsed X-ray imaging test, the value was 6.1%. This finding suggests that for shaped-charge liners made of the same material, their forming process affect jet formation and its parameters. Concerning jet velocity alone, the supercooled liquid-phase high-rheological-rate formation process outperforms the vacuum die casting process.

6. Conclusions

- The numerical simulation results showed that the jet velocity of Zr-based amorphous alloy liners was in gradient descent from the head to the tail. It was also found that the jet's head velocity reached the maximum of 8026 m/s at 12 μs and then slowly decreased during the period of 12–40 μs.
- The average jet velocity measured by the copper foil target velocity-measuring test was 7177 m/s, but the value given by the pulsed X-ray imaging test was 6913 m/s.
- The formation process of liners has effects on the formation and parameters of shaped-charge jets. Specifically, the Zr-based amorphous alloy liner formed by the supercooled liquid high-rheological-rate formation process delivered a jet velocity 6.5% higher than that formed by the vacuum die casting process.

Author Contributions: Investigation, visualization and writing-original draft, P.C. and J.X.; methodology and supervision, X.G.; resource and project administration, Y.Y.; funding acquisition, J.W.; data curation, L.C.; writing-reviewing and editing, C.L. All authors have read and agreed to the published version of the manuscript.

Funding: This research was funded by the Scientific Research Project of Army Weapons and Equipment (Grant No LJ20202A020403) and the APC was funded by Army Engineering University of PLA.

Institutional Review Board Statement: Not applicable.

Informed Consent Statement: Not applicable.

Data Availability Statement: Not applicable.

Acknowledgments: The authors appreciated the precious comments and suggestions of the editors and reviewers.

Conflicts of Interest: The authors declare no conflict of interest.

References

1. Allison, F.E.; Vitali, R. *A New Method of Computing Penetration Variables for Shaped Charge Jet*; Army Ballistic Research Laboratory: Aberdeen Proving Ground, MD, USA, 1963.
2. Wang, C.; Ding, J.X.; Zhao, H.T. Numerical Simulation on Jet Formation of Shaped Charge with Different Liner Materials. *Def. Sci. J.* **2015**, *65*, 279–286. [CrossRef]
3. Wang, Z.; Jiang, J.W.; Wang, S.Y.; Liu, H. Jet foromation and penetration study of double-layer shaped charge. *J. Energ. Mater.* **2018**, *36*, 152–168. [CrossRef]
4. Fedorov, S.V.; Ladov, S.V.; Nikol'skaya, Y.M.; Baskakov, V.D.; Baburin, M.A.; Kurepin, A.E.; Gorbunkov, A.A.; Pirozerskii, A.S. Formation of a high-velocity particle flow from shaped charges with a liner consisting of a hemisphere and a degressive-thickness cylinder. *Combust. Explos. Shock Waves* **2017**, *53*, 479–482. [CrossRef]
5. Hayes, G.A. Linear shaped-charge (LSC) collapse model. *J. Mater. Sci.* **1984**, *19*, 3049–3058. [CrossRef]
6. Xiao, Q.Q.; Huang, Z.X.; Zu, X.D.; Jia, X. Influence of frift velocity and distance between jet particles on the penetration depth of shaped charges. *Propell. Explos. Pyrotech.* **2016**, *41*, 76–83. [CrossRef]
7. Chase, J.B.; Kuklo, R.M.; Shaw, L.L.; Carter, D.L.; Baum, D.W. *High Resolution Diagnostics of a Linear Shaped Charge Jet*; No. UCRL-JC-133098; Lawrence Livermore National Lab. (LLNL): Livermore, CA, USA, 1999.
8. Wang, C.; Xu, W.L.; Steeve, C.K.Y. Penetration of shaped charge into layered and spaced concrete targets. *Int. J. Impact Eng.* **2018**, *112*, 193–206. [CrossRef]
9. Jia, X.; Huang, Z.X.; Zu, X.D.; Gu, X.H.; Zhu, C.S.; Zhang, Z.W. Experimental study on the performance of woven fabric rubber composite armor subjected to shaped charge jet impact. *Int. J. Impact Eng.* **2013**, *57*, 134–144. [CrossRef]
10. Salih, S.; Oğuzhan, A.; Mehmet, S.Y. Experimental investigations on aluminum shaped charge liners. *Procedia Eng.* **2013**, *58*, 479–486.
11. Liu, J.; Chen, X.; Du, Z.H. A study on the surface overpressure distribution and formation of a double curvature liner under a two-point initiation. *Def. Technol.* **2022**, *18*, 148–157. [CrossRef]
12. Gilbert, C.J.; Ager, J.W.; Schroeder, V.; Ritchie, R.O. Light emission during fracture of a Zr-Ti-Cu-Ni-Be bulk metallic glass. *Appl. Phys. Lett.* **1999**, *74*, 3809–3811. [CrossRef]
13. Wei, H.Y.; Yoo, C.S. Kinetics of small single particle combustion of zirconium alloy. *J. Appl. Phys.* **2012**, *111*, 506–513. [CrossRef]
14. Han, W.; He, Y.; Wang, C.T.; Ji, C.; He, Y.; Guo, Z.P. Experimental study on the damage ability of reactive fragments fabricated by Zr-based metallic glass (an environment perspective). *Ekoloji* **2019**, *28*, 4885–4890.
15. Wang, C.T.; He, Y.; Ji, C.; He, Y.; Han, W.; Pan, X.C. Investigation on shock-induced reaction characteristics of a Zr-based metallic glass. *Intermetallics* **2018**, *93*, 383–388. [CrossRef]
16. Laszlo, J.K.; William, P.W. Investigation of a bulk metallic glass as a shaped charge liner material. In Proceedings of the 23rd International Symposium on Ballistics, Tarragona, Spain, 16–20 April 2007; pp. 269–274.
17. Cui, P.; Wang, D.S.; Shi, D.M.; Gao, X.B.; Xu, J.Q.; Zhen, J.W. Investigation of penetration performance of Zr-based amorphous alloy liner compared with copper. *Materials* **2020**, *13*, 912. [CrossRef]
18. Cui, P.; Shi, D.M.; Zhang, Y.L.; Wang, D.S. Numerical simulation and experimental study on jet forming and penetration performance of Zr-based amorphous alloy liner. *Eng. Lett.* **2021**, *29*, 151–157.
19. Chen, L.; Zu, X.D.; Huang, Z.X.; Xiao, Q.Q.; Han, W. Study on jet forming of Zr-based amorphous alloy liner. *J. Ballist.* **2022**, *34*, 65–71.
20. Wang, H.F.; Guo, H.G.; Geng, B.Q.; Yu, Q.B.; Zheng, Y.F. Application of PTFE/Al Reactive Materials for Double-Layered Liner SC. *Materials* **2019**, *12*, 2768. [CrossRef] [PubMed]
21. Guo, H.G.; Zheng, Y.F.; Yu, Q.B.; Ge, C.; Wang, H.F. Penetration behavior of reactive liner shaped charge jet impacting thick steel plates. *Int. J. Impact Eng.* **2019**, *126*, 76–84. [CrossRef]
22. Shi, Y.X.; Shi, D.M.; Li, W.Z.; Yu, Z.T.; Shang, C.M. Study on JH-2 model of the ZrCuNiAlAg bulk amorphous alloy. *Explos. Shock Waves* **2019**, *39*, 093104.
23. Han, J.L.; Chen, X.; Du, Z.H.; Fu, H.M.; Huang, D.W. Design and penetration of a new W-particle/Zr-based amorphous alloy composite liner. *J. Braz. Soc. Mech. Sci.* **2020**, *42*, 364. [CrossRef]
24. Yi, J.Y.; Wang, Z.J.; Yin, J.P.; Zhang, Z.M. Simulation study on expansive jet formation characteristics of polymer liner. *Materials* **2019**, *12*, 744. [CrossRef] [PubMed]
25. Guo, H.G.; Xie, J.W.; Wang, H.F.; Yu, Q.B.; Zheng, Y.F. Penetration behavior of high-density reactive material liner shaped charge. *Materials* **2019**, *12*, 3486. [CrossRef]
26. Bai, X.; Liu, J.X.; Li, S.K.; Lv, C.C.; Guo, W.Q.; Wu, T.T. Effect of interaction mechanism between jet and target on penetration performance of shaped charge liner. *Mater. Sci. Eng. A* **2012**, *553*, 142–148.